Detection of Thunderstorm Using Indian Navigation Satellite NavIC

Saurabh Das, *Senior Member, IEEE*, Soumen Datta, and Ashish K. Shukla

***Abstract*— Navigation satellites provide a good opportunity to monitor both ionospheric and tropospheric conditions by using propagation delays in the L-band signal. However, the availability of S-band frequency in the Indian Regional Navigation Satellite System, Navigation with Indian Constellation (NavIC), provides a unique opportunity to utilize signal strength for monitoring thunderstorms. This article, for the first time, demonstrates that NavIC satellite signal strength measurements can be used to detect thunderstorms. A dynamic time warping technique has been used to detect the presence of thunderstorm cloud systems. The method has been tested with several case studies in Kolkata using one-year measurements. The results indicate suitability of such techniques for monitoring and forecasting of thunderstorms using a navigation satellite.**

***Index Terms*— Dynamic time warping (DTW), Navigation with Indian Constellation (NavIC), S-band, signal strength, thunderstorm.**

I. Introduction

PRECIPITABLE water vapor (PWV), a key weather parameter, plays an important role in weather forecasting as well as poses a significant challenge for satellite-based navigation applications. The direct role of water vapor in thunderstorm and heavy precipitation is one of the many intriguing aspects, and the measurements of the same are used as a precursor for predicting extreme weather events. The use of troposphere-induced signal delay in navigation satellite systems, such as GPS, is now-a-days widely used in estimating the PWV for numerical weather prediction and various remote sensing applications due to its all-weather operations which was first proposed by Bevis *et al.* [1]. Establishment of worldwide GPS/Global Navigational Satellite System (GNSS) network and remarkable progress in atmospheric water vapor estimation algorithms from these signals have been achieved during the last two decades [2]–[9].

In comparison to GPS and other existing navigation constellations, the recently launched Indian navigational satellite system, Navigation with Indian Constellation (NavIC), not only increases the number of available ray paths over India but also provides additional measurements in the S-band for the first time. This is a unique characteristic of NavIC; other constellations are working predominantly in the L-band. This actually provides a rare opportunity to utilize the relative signal strengths variation at two widely spaced bands (L and S) to monitor the thunderstorm systems directly, instead of conventional approaches by measuring water vapor. So far signal strength variation from navigation satellites has been utilized in several aspects such as the detection and mitigation of multipath effect [10]–[12], sensing ground moisture [13]–[15], and ocean remote sensing such as determination of sea level or tide gauge [16]–[19]. The well-known application of signal strength observable is in GNSS reflectometry (GNSS-R) by using the GNSS scattered signal of opportunity [20]. Aircraft-based GNSS-R bistatic radar is a popular GNSS-R approach for various ocean remote sensing [21], [22]. The newly launched Cyclone Global Navigation Satellite System (CYGNSS) provides another good opportunity for various ocean remote sensing such as cyclone monitoring [23], [24], wind speed retrieval [25], and measurement of soil moisture [26]. All these applications are based on the received signal directly from the satellite along with reflected from nearby surfaces. However, this is the first attempt to study the thunderstorm system using the direct satellite signal strength indicated by $C/N0$.

Though the attenuation due to water vapor, cloud, or rain (i.e., atmosphere) on the L- or S-bands is very less, it can still be differentiated due to the wide separation of these two frequencies. Signal strength attenuation in 2.1-GHz radio wave propagation, due to rain, was first investigated by Michalek *et al.* [27]. This article has proposed a novel approach using differential signal strength measurements to detect this tropospheric contribution, particularly during thunderstorm.

Some case studies using measurements from NavIC at Kolkata, India (22.65 N, 88.38 E) are presented here. It was found that the strength variations of the NavIC signal correlated with records from Doppler radar of the India Meteorological Department (IMD), Kolkata, which was monitoring the cloud structure during thunderstorms. This finding indicates that the NavIC signals can be used for measuring the movement of a large cloud system. A dynamic time warping (DTW) technique is further used to efficiently detect the thunderstorm system. The results indicate the potential application of NavIC system for early warning system development.

Manuscript received May 24, 2019; revised October 11, 2019; accepted November 29, 2019. Date of publication January 7, 2020; date of current version April 22, 2020. This work was supported in part by the Space Application Centre, Indian Space Research Organization (ISRO) through the NavIC-GAGAN Project Scheme (NGP-1) and in part by the DST-INSPIRE Faculty Scheme under Grant DST/INSPIRE/04/2014/002492. *(Corresponding author: Saurabh Das.)*

S. Das and S. Datta are with the Discipline of Astronomy, Astrophysics and Space Engineering, IIT Indore, Indore 452017, India (e-mail: das.saurabh01@gmail.com).

A. K. Shukla is with the Space Applications Centre, Indian Space Research Organization (ISRO), Ahmedabad 380015, India.

Color versions of one or more of the figures in this article are available online at http://ieeexplore.ieee.org.

Digital Object Identifier 10.1109/TGRS.2019.2960035

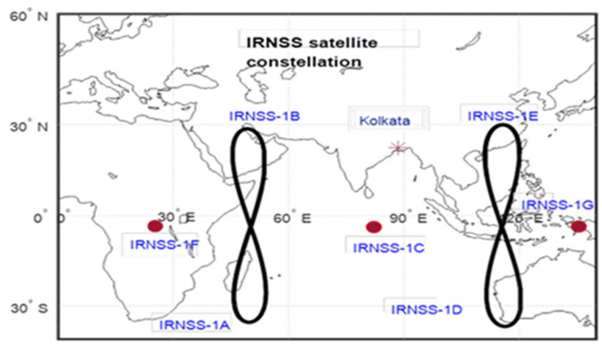

Fig. 1. NavIC satellites.

II. System Description

The Indian Regional Navigation Satellite System (IRNSS) with an operational name of NavIC is a regional navigation satellite system. It provides real time positioning and timing services with its seven satellites' constellation. Four of these seven satellites are geosynchronous (i.e., not in equatorial plane and having orbital movement though time synchronizes with the rotation of the Earth) and the rest are geostationary (i.e., apparently fixed in orbit and in equatorial plane). The constellation diagram of NavIC system is shown in Fig. 1. NavIC facilitates standard positioning service and precision positioning service operated at two widely separated frequencies, in L5-band (1176.45 MHz) and S1-band (2492.028 MHz).

The navigation data for studies described here obtained from an IRNSS/GPS/SBAS SPS user receiver (make: ACCORD) installed on the roof top of the Indian Statistical Institute, Kolkata. This is a dual frequency GNSS receiver which is capable of acquiring and tracking NavIC (dual frequency L5- and S1-bands), GPS (L1 C/A), and SBAS (GAGAN) signals. Data have been logged with 1-Hz resolution. Continuous observations of one year from November 2017 to November 2018 have been considered for the study.

Doppler radar images from IMD were used for tracking the movement of thunderstorm systems. This S-band Doppler weather radar (DWR) provides information regarding reflectivity (Z), radial velocity (V), and spectral width (ω) in both plan-position indicator (PPI) and range height indicator (RHI) modes. Based on these parameters and standard algorithms, various products of practical utility for issuing forecasts and warnings are generated (http://www.imd.gov.in). Among various data products provided by this DWR, the MAX (Z) or maximum (reflectivity) product has been used in this study as it can efficiently indicate cloud movement.

The study location, Kolkata, is situated in the lower Ganges Delta of eastern India. The city has a tropical wet and dry climate and gets most of its rain during June–September due to the south-east monsoon wind flow. The study location is very rich from the observational point of view because of the frequent weather extremes. Nor'westers is one such extreme event which occurs during the month of March to May over Eastern India, causing considerable damages to life and property. Nor'westers is specially accompanied by strong squalls, lightning, and sometimes by hail [30].

III. Methodology

GNSS observables such as pseudorange, carrier phase, or the Doppler frequency are commonly used in GNSS atmospheric applications. However, in this article, instead of these commonly used observables, the signal strength related to the value of $C/N0$ is considered for the detection of thunderstorm system. The $C/N0$ indicates the carrier-to-noise ratio and is indicative of the channel impairment if the path geometry and other conditions remain unchanged. For a static receiver, it then becomes a function of only propagation effects due to both ionosphere and troposphere.

The $C/N0$ values have both slow and rapid fluctuations which are caused by several factors such as ionospheric scintillation, troposphere, multipath, and elevation angle. Ionospheric contribution is more prominent on the L-band signal than that in the S-band. So any ionospheric total electron content (TEC) variation (particularly scintillation) will degrade the L-band signal more than the S-band one. Moreover, the scintillation effect can be easily identified as the rapid fluctuation of the signal. The multipath phenomenon, however, affect both the signals in a similar way as the elevation and azimuth are the same at these two frequencies as well as the surrounding environment of the receiver. The relative degradation of $C/N0$ in the L- and S-band signals will essentially then indicate the atmospheric and ionospheric contributions. To separate out the tropospheric contributions from the ionospheric part is then based on two criteria: we need to look for signatures where the S-band is more degraded than the L-band and focus only on slow moving components.

For this article, three similarity measure techniques are investigated, namely, simple template matching, Pearson correlation, and DTW technique. First, the outlier data points (spikes) were removed with a low pass filter. These outliers arise due to instrument or other effects and are not necessarily related to the propagation characteristics.

A. Simple Template Matching in S-Band

One of the primary hypotheses in this work is that the relative change between the S- and L-bands can detect only the thunderstorm. However, it is worth investigating whether only S-band information can be used for this purpose. As multipath remains unchanged for a static receiver, simple template matching in the S-band between consecutive rainy (R) and nonrainy (NR) days also indicates the thunderstorm. Hence, the template matching between two consecutive days is applied with different time windows (60, 30, and 1 min) on a 18-day-long time series which involve two thunderstorm days in between.

B. Correlation Analysis

Next, the Pearson correlation analysis has been done for both the L- and S-band signals between two consecutive days. Correlation is calculated for different time windows (60, 30, and 1 min). Then the difference between correlations of two consecutive pair of days is compared. This approach is tested on the same 18-day-long time series.

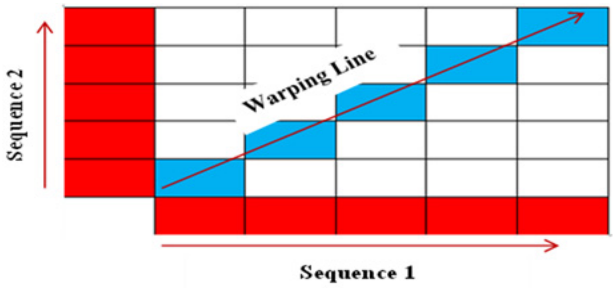

Fig. 2. Schematic of the DTW technique.

C. DTW Algorithm

Lastly, a DTW algorithm is used between two temporal sequences of the L- and S-bands. The data have been averaged over 1 min for DTW study. The DTW calculation is carried out for all instances over a specified time period and then restarted for the next time span. In each calculation, the warping line (WL) is obtained by considering ten instances of the second time series. DTW matches patterns of two temporal sequences and has been widely utilized in speech recognition. It finds the closest match between two sequences by using their cumulative difference. Here, two temporal sequences are taken and the value of each index in a sequence is matched with values of all indices of another. For this article, a window of ten instances has been used to minimize the time complexity. Instead of matching all indices it matches up to ten indices of the second sequence with every index of the first sequence. The detailed description of the DTW algorithm can be found in [28] and [29], a short description of the algorithm is provided in the following paragraphs.

Two temporal sequences of observation can be arranged along the two sides of a grid, i.e., one at the bottom and another along the left-hand side as shown in Fig. 2 (marked in red). Both the sequences start from the bottom left corner of the grid. The distances, finding the difference of corresponding elements of the two sequences, are placed inside each cell of the grid. This measured distance is a dynamic recurrence relation based on the cumulative distance between the two points of interest which can be stated as follows:

$$\pounds(i+1, j+1) = \delta(i+1, j+1) + \min[\pounds(i, j+1), \pounds(i, j), \pounds(i+1, j)] \quad (1)$$

where $\pounds\ (i,\ j)$ defines the values of each grid points, and $\delta(i,\ j)$ is the measured distance between two points of sequences.

Warping path is then computed by backtracking the minimum of the accumulated distance matrix and is helpful for pattern matching. However, for our case, it was necessary to match the timing information as well and hence a slight modification of this technique is done here. Instead of a warping path, a WL is computed by considering the leading diagonal terms of the grid in order to preserve the timing information (marked in blue in Fig. 2). For example, the nth difference will contain the cumulative sum of minimum neighborhood values in $(n-1)$ to nth point differences. This cumulative distance-based recurrence relationship automatically reduces the higher frequency rippling effects present in the signal strength due to the ionospheric scintillation, multipath, or other instrumental errors, and enhances slowly moving changes by a very small amount due to the tropospheric effect. Since DTW measures the index-wise difference between (i.e., at the same time instant two time-series cumulatively, this small attenuation spanning over a long duration is amplified to a comprehensible level.

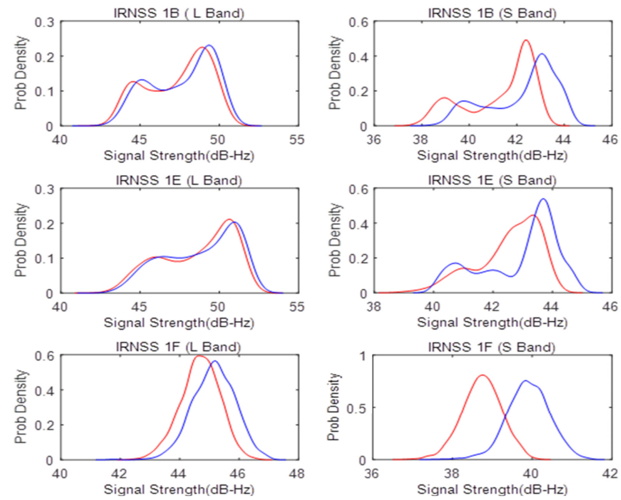

Fig. 3. L- and S-band signal strength variation of two months. June is indicated in red, and November is indicated in blue.

IV. Results and Discussion

A. Seasonal Variation of Signal Strength

Signal strength may depend on several factors as already mentioned. Before utilizing the signal strength variation for detecting thunderstorm, the seasonal variation has been studied. In Fig. 3, the probability distribution of signal strength variation of two months from two different seasons has been shown for three different satellites. June indicates the monsoon season (increased water vapor in the atmosphere) and November represents winter season (dry weather). The signal strength variations in the L-band are very similar to each other. However, one can note that there are significant differences of signal strength in the S-band between these two months.

There is a left shift of S-band signal strength for the month of June comparative to November which is not prominent for L-band signal strength. This clearly indicates that S-band signal strength is affected more during the month of June in comparison to the month of November.

Since the L-band does not show much variation, we can neglect the change in the multipath effect. The ionospheric activities during these two months are also very similar with respect to disturbance storm time (Dst) and Kp indices [http://wdc.kugi.kyoto-u.ac.jp/wdc/Sec3.html]. Dst index is a measure of Earth's magnetic activity and computed from the measurements of a network of near-equatorial geomagnetic observatories. The Kp-index also indicates the global geomagnetic activity and is based on 3-h measurements by ground-based magnetometers spread all over the world.

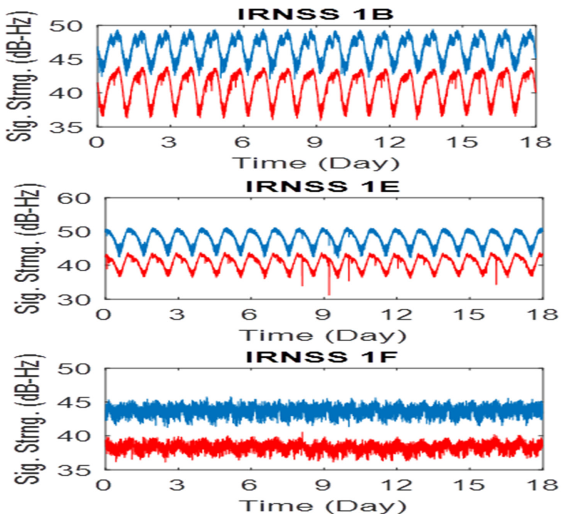

Fig. 4. L- and S-band signal strength variation of 18 days. L-band is indicated in blue, whereas S-band is indicated in red.

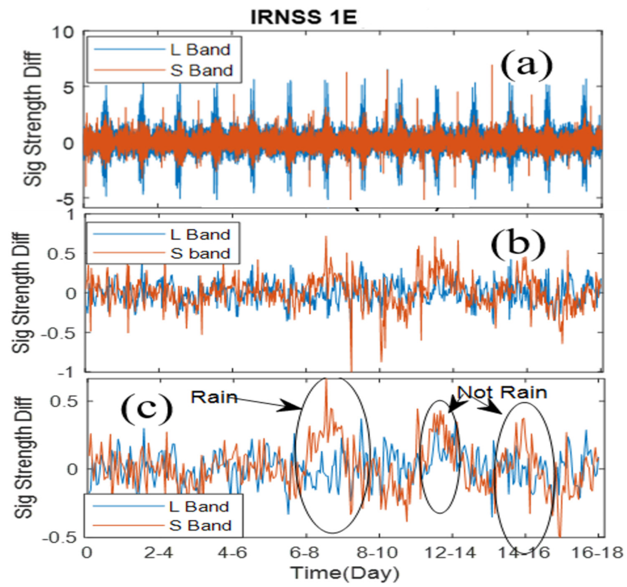

Fig. 5. Template matching between two consecutive days in S- and L-bands with a resolution of (a) 1, (b) 30, and (c) 60 min.

Presence of large numbers of cloud system due to the monsoon makes the month of June distinct from November. It can be concluded that the apparent cause of S-band signal strength variation, which is negligible in the lower frequency band (L-band), is primarily due to troposphere.

B. Case Studies

Here, we present three case studies to show the potential of NavIC system in detecting the thunderstorms. The 1st case study focuses on the signature of signal strength variation obtained during the development of a cloud system over the study location and the advantage and disadvantages of previously mentioned three techniques in detecting the same. The 2nd case study focuses on detecting the movement of the cloud system based on DTW technique while 3rd case study focuses on the detection of two consecutive cloud system.

1) Case Study 1 [Long Term Signal Strength Variation and Signature of Rainy Day (December 1–18, 2017)]: The time series considered here contains 18-day-long measurements which represent two rainy days at the center with eight NR days before and after the rain event. The nature of signal strength variation of the L- and S-bands is shown in Fig. 4. The signal strength variation does not show any visible difference during the rainy days in comparison to other NR days because of the very small magnitude of tropospheric contribution. Hence, to detect the tropospheric effect, first simple template matching is used as discussed next.

a) Template matching: Since the multipath effect remains constant for static receiver, first a simple template matching has been performed on signal strength difference between two consecutive days separately for the L- and S-bands. This is shown in Fig. 5. Instead of 1-s signal, the signal has been averaged over three different windows of 1, 30, and 60 min. The 1- and 30-min analyses did not show any noticeable signature during the rain event, but the 60-min analysis successfully captured the signature due to an increase in signal strength difference. However, one can also note that there are increased signal strength differences in two other instances also which do not correspond to the rainy days. Although the increase in signal strength difference in the S-band is more than the L-band during a rainy day, the anomalous increases are observed simultaneously in both the S- and L-bands in almost the same magnitude. Another important observation is that the simple template matching is unable to detect the rainy day signature with coarse temporal resolution and hence may not be suitable for tracking a cloud system.

b) Correlation analysis: Next, the correlation analysis has been done with the same three different time windows, i.e., with 1, 30, and 60 min. The correlation is estimated between each pair of consecutive days spanning 18 days. Thereafter, the differences between consecutive pairs of correlations are compared. Fig. 6(a)–(c) shows the results of correlation analysis with different time window size. It can be noted that the 1-min analysis does not show any distinct signature during rain, however, the 30-min analysis is now able to identify the rain event though the signature is not very clear. The 60-min analysis also shows a distinct signature during rain event. Therefore, it is clear from the analysis that the tropospheric disturbances are well captured by correlation analysis of the signal strength difference. However, the temporal resolution of this detection method is still poor. So, it is imperative to use a technique which can detect the tropospheric events with a better resolution.

c) DTW technique: Next, DTW is applied separately on the L- and S-bands as well as on the difference of L- and S-bands between two consecutive days. Then the WLs differences of two consecutive pair of days are computed. This is shown for two different satellites in Fig. 7. It is to be noted here that as DTW is a cumulative technique, it has to be restarted after some specific time interval. As the focus of this case study 1 is just to detect the rainy days, the DTW calculation is restarted every 24 h. Only the results

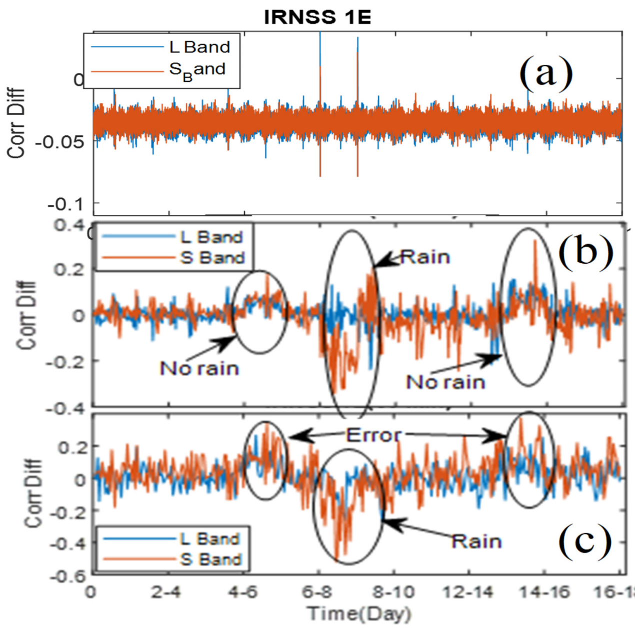

Fig. 6. Correlation between two consecutive days in S- and L-bands with time windows of (a) 1, (b) 30, and (c) 60 min.

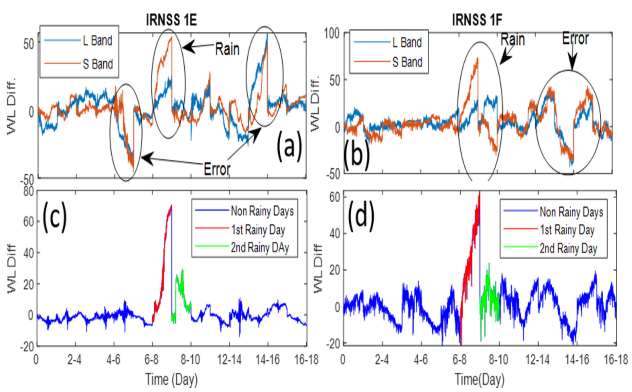

Fig. 7. Variation of WLs between two consecutive days for L- and S-band signal strength separately for (a) IRNSS IE satellite and (b) IRNSS 1F satellite. (c) and (d) WL differences between L- and S-bands for consecutive days.

of DTW with 1-min resolution are shown here as it has the ability to detect the rain signature. Moreover, the increase in WL difference is similar for both the L- and S-bands during NR days as can be seen in Fig. 7(a) and (b). Hence, the relative changes in WL between the L- and S-bands can effectively help in reducing false detection as shown in Fig. 7(c) and (d). A certain rise of WL (marked in red) difference is observed during the rainy day, December 9, 2017. Similar behavior is noted on the next rainy day, December 10, 2017 (marked in green), though the magnitude of the variation is less. The first difference corresponds to one NR and one rainy day, whereas the second one represents the difference of two rainy days. This indicates the suitability of the DTW technique for detecting the rain events with an improved resolution.

2) Case Study 2 [Monitoring a Thunderstorm System (April 12, 2018)]: A thunderstorm day (April 12, 2018) is considered for this purpose. The thunderstorm system developed on the said day and gradually moved over the observation point. Two clear days (April 10 and 11, 2018) are chosen for a comparative analysis. The whole day is segmented for a detailed study into three different time sessions of 8-h duration. As DTW is cumulative technique, the very purpose of dividing each day into three parts is just to avoid the accumulation of the difference throughout the day, so that the effect can be seen clearly. Session 1 indicates a time span of 0–8 UTC, session 2 indicates 8–16 UTC, and session 3 indicates 15–23 UTC. DTW is applied between signal strength of the L- and S-bands for every session of each day and the obtained WLs are compared between the same session of the two consecutive days [i.e., between two NR days (April 10 and 11, 2018) and between rainy and its consecutive NR day (April 11 and 12, 2018)]. This WL difference for every session of three satellites are shown in Fig. 8. It is observed that during all three sessions there are no significant deviations in the NR–NR WL difference while rainy–NR (R–NR) WL difference shows significant variations. It is observed that during session 1, R–NR line of IRNSS 1C has deviated from the zero level which is not seen for IRNSS 1B and IRNSS 1E. In session 2, it can be seen that R–NR line has deviated for all of the satellites but this deviation in IRNSS 1B and 1C started before the IRNSS 1E. Whereas in session 3, R–NR line of only IRNSS 1E and 1C deviated significantly.

To understand the nature of this variation, IMD Doppler radar data of the event are also shown in Fig. 8. It is clearly visible from the NavIC orbital constellation (shown in Fig. 1) and Doppler radar cloud coverage picture that the cloud has moved from the direction of IRNSS 1C. This finds good agreement with the WL variation shown in Fig. 8. The starting time of such a deviation corresponded well with the cloud overcast as IRNSS 1B and 1C are affected earlier than IRNSS 1E. IRNSS 1E has only been affected after the cloud moved over the study location.

3) Case Study 3 [A Case Study of Two Cloud Systems From Two Different Directions (June 20, 2018)]: Here again three consecutive days are considered. The first two days are NR whereas, the third day is a rainy one. The full day span is again divided into three consecutive time segments. Here, for each time segment, the WL between L- and S-band signal strength is computed for the three days separately. Then the comparative analyses (Fig. 9) are performed, first, between the two consecutives NR days and second, between the NR and rainy days.

Fig. 9(a) shows the WL comparison during first session (0–8 h) of the day along with the cloud image of Doppler radar of a rainy day during this time period. The blue line shows the WL comparison of two NR days and the red line shows the WL comparison between the NR day and its consecutive rainy day. It is evident from the Doppler radar images that there is no such large cloud system during this session. This is also reflected in our comparison lines. Small day-to-day differences still exist, but these are regular in nature.

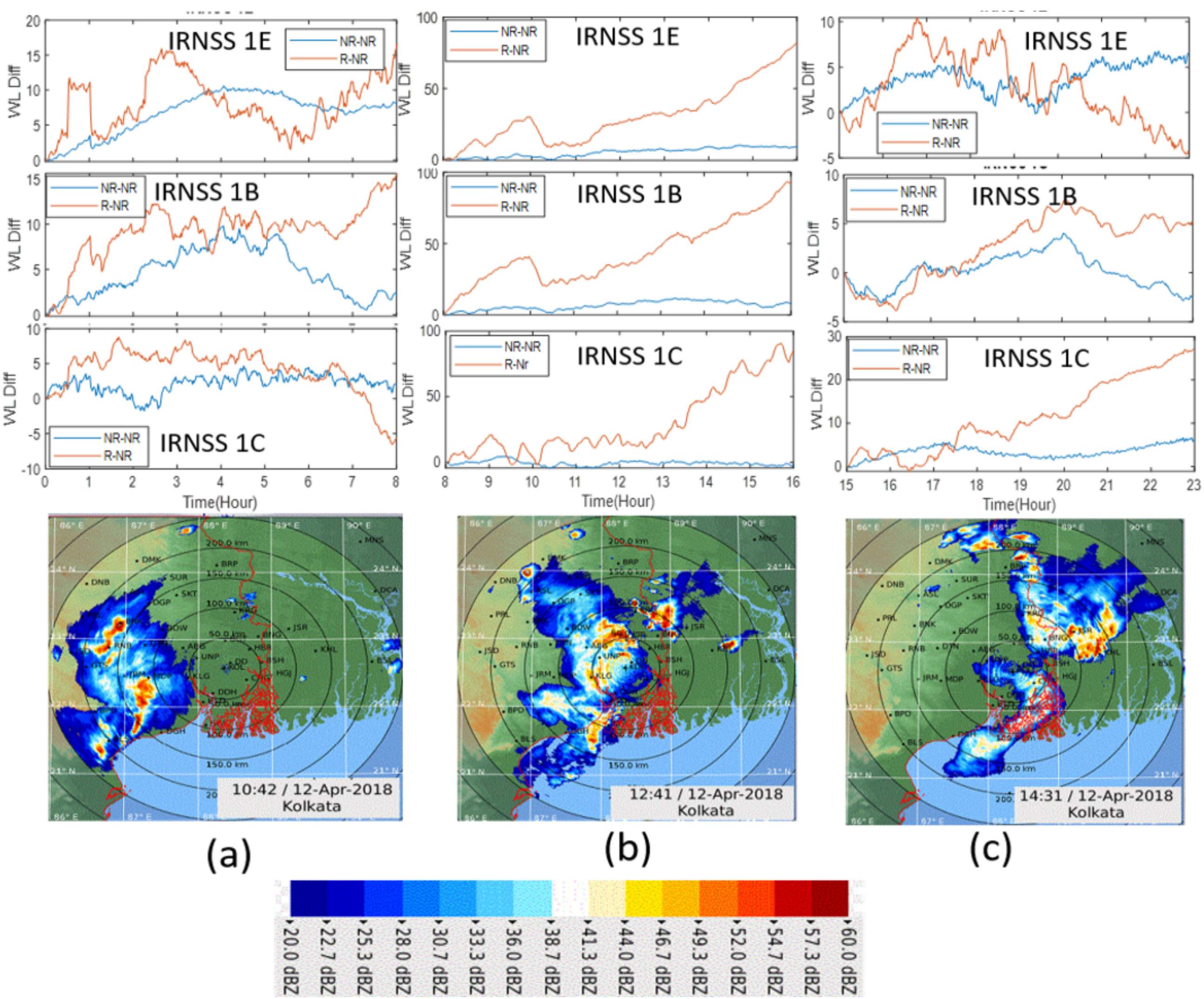

Fig. 8. WL variation of three sessions of the day and movement of the cloud system as observed by the Doppler radar cloud imagery. (NR: nonrainy day and R: rainy day). (a) 0–8 UTC. (b) 8–16 UTC. (c) 15–23 UTC.

The same study is repeated for the second session of the day. A clear difference between NR–NR comparison line and rainy–NR comparison line can be seen [Fig. 9(b)].

This large variation could have resulted either from a high value of rainy day WL or low value of NR day WL. However, from the low WL difference that is indicated in a two NR day comparison, it can be assumed that there is no significant change in two NR days. So the large variation in WL difference between rainy and NR day must be due to the presence of rainy day. Since, the WL only indicates the index wise comparison (i.e., at the same instant) between two time series, the high value of rainy day WL clearly suggests the possibility of S-band signal strength degradation. It can be noted from Doppler radar imagery that a cloud system has developed over the study location during this session of the day which supports our assumption of cloud coverage effect on the S-band signal strength variation.

The mentioned cloud system seems to disappear during the final session (15–23 h) of the day, whereas a shallow cloud system developed [Fig. 9(c)]. Interestingly, the second cloud cover seemed to affect the line-of-sight of only two satellites, IRNSS 1C and 1B. This is clearly reflected in the WL study as well. On the other hand, the effect on 1E has reduced as a result of disappearance of the previous cloud system developed during the earlier session.

V. Discussion

Both simple pattern matching and correlation analysis indicate that the S-band signal is affected by a thunderstorm system. However, to uniquely identify the thunderstorm signature, a comparison with the L-band is essential to filter out other effects. The correlation analysis or template matching cannot detect the thunderstorm in high resolution and hence the DTW method is adopted. As the DTW technique measures the cumulative distance between each of the two corresponding points of two time series, the small differences get amplified in this process. The proposed method is able to detect the

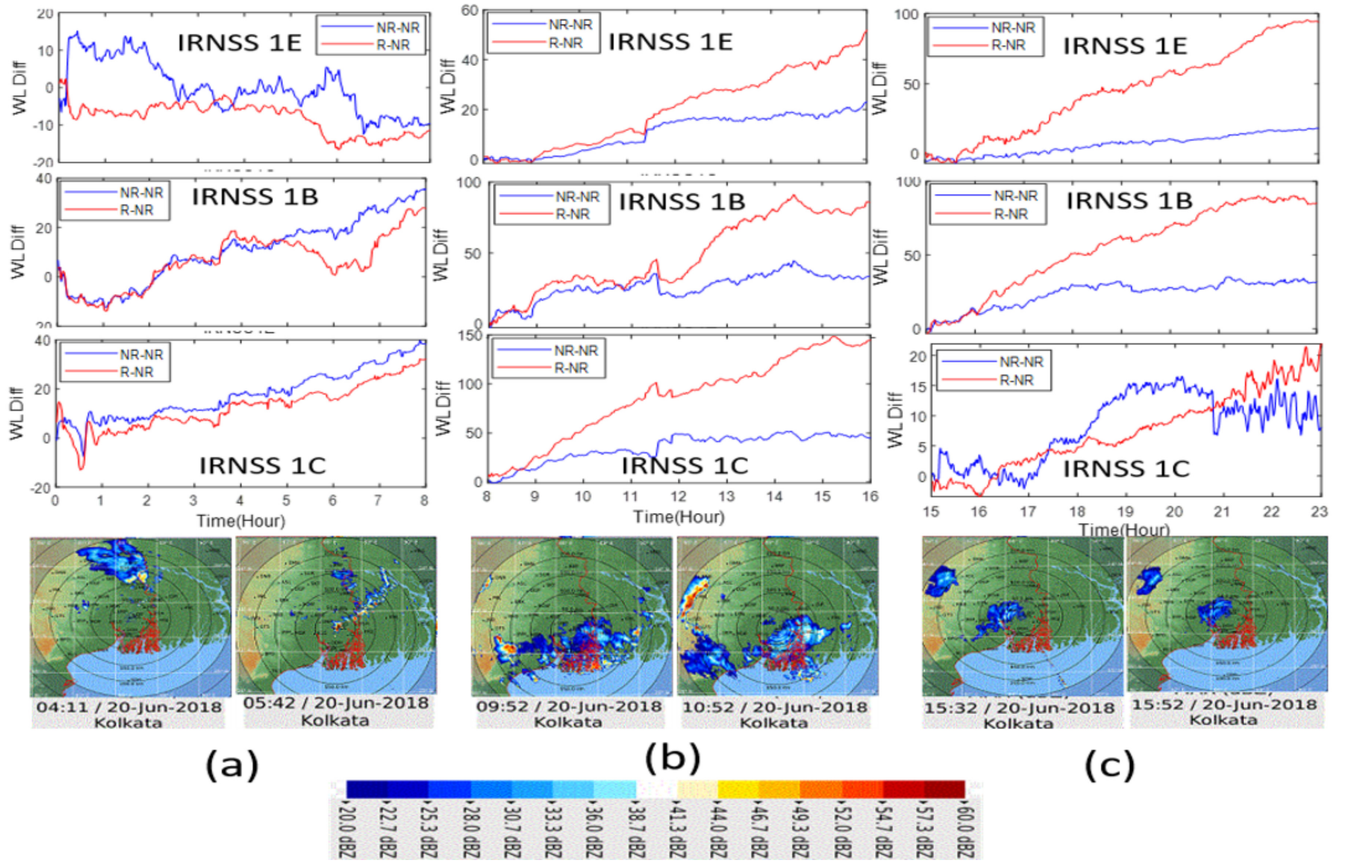

Fig. 9. WL variation of three sessions of the day and evolution of two cloud systems as observed by the Doppler radar cloud imagery. (NR: nonrainy day and R: rainy day). (a) 0–8 UTC. (b) 8–16 UTC. (c) 15–23 UTC.

thunderstorms with 1-min temporal resolution in the long time series of S- and L-band signal strength. To further study the capability of the present method, two other case studies are carried out. In case study 2, the proposed technique is used to detect the movement of the cloud system whereas in case study 3, two cloud systems are detected. The proposed technique requires resetting the WL after some time as the technique enhances the difference between L- and S-band signals cumulatively. This time gap depends on the frequency of the event that is being detected. At present, this is done arbitrarily at a fixed time interval and is the reason why in case studies 2 and 3, we divided the whole day into 8-h session, whereas in case study 1, it is 24 h. Automatic resetting of WL after the thunderstorm will be essential for practical implementation and will be addressed in the future study. It should be noted, however, in all the cases the WLs are obtained between the same time period of consecutive days.

The multipath effect, which is rather a serious issue only in low elevation angle less than 23° for the present location, is automatically taken care of in the present method as multipath is almost invariant for two consecutive days for a static receiver and we are only interested in the relative changes between two consecutive days. Furthermore, the present technique is equally applicable during ionospheric scintillation which essentially means a rapid fluctuation of the signal. As DTW enhances the slow variations or the trends in the signal, the thunderstorm effect can thus be detected under ionospheric scintillation. It should, however, be noted that we have not been able to test this in real time since during the observation period there are no scintillation events observed, as we are in solar minima period.

VI. Conclusion

The comparative analysis of signal strength between the L- and S-bands of NavIC system shows that there is a clear impact of tropospheric phenomenon like heavy rain or dense cloud cover on S-band signal. This is evidenced by its relatively large signal strength degradation in the S-band over the L-band under the same climatic conditions. Accordingly, a comparative DTW approach is developed to detect this extra degradation of the S-band signal due to weather phenomena. The application of DTW facilitates differentiation of a small degradation in the S-band signal. The method has been tested with a number of events over Kolkata. Results indicate that NavIC can be used to develop a monitoring system for such kind of extreme weather events.

Acknowledgment

The authors would like to thank Dr. K. Gopalan, Space Applications Centre, Indian Space Research Organization (ISRO), Ahmedabad, India, for his technical guidance. They would also like to thank the Indian Meterological Department, Kolkata, India, for providing the Doppler radar images.

References

[1] M. Bevis, S. Businger, T. A. Herring, C. Rocken, R. A. Anthes, and R. H. Ware, "GPS meteorology: Remote sensing of atmospheric water vapor using the global positioning system," *J. Geophys. Res.*, vol. 97, no. D14, p. 15787, 2012.

[2] M. Bevis *et al.*, "GPS meteorology: Mapping zenith wet delays onto precipitable water," *J. Appl. Meteorol.*, vol. 33, no. 3, pp. 379–386, 1994.

[3] C. Rocken *et al.*, "Analysis and validation of GPS/MET data in the neutral atmosphere," *J. Geophys. Res.*, vol. 102, no. D25, pp. 29849–29866, Dec. 1997.

[4] P. Fang, M. Bevis, Y. Bock, S. Gutman, and D. Wolfe, "GPS meteorology: Reducing systematic errors in geodetic estimates for zenith delay," *Geophys. Res. Lett.*, vol. 25, no. 19, pp. 3583–3586, 1998.

[5] T. Ning and G. Elgered, "Trends in the atmospheric water vapor content from ground-based GPS: The impact of the elevation cutoff angle," *IEEE J. Sel. Topics Appl. Earth Observ. Remote Sens.*, vol. 5, no. 3, pp. 744–751, Jun. 2012.

[6] Y. Yao and Q. Zhao, "Maximally using GPS observation for water vapor tomography," *IEEE Trans. Geosci. Remote Sens.*, vol. 54, no. 12, pp. 7185–7196, Dec. 2016.

[7] X. Li *et al.*, "Multi-GNSS meteorology: Real-time retrieving of atmospheric water vapor from BeiDou, Galileo, GLONASS, and GPS observations," *IEEE Trans. Geosci. Remote Sens.*, vol. 53, no. 12, pp. 6385–6393, Dec. 2015.

[8] W. Ding, F. N. Teferle, K. Kazmierski, D. Laurichesse, and Y. Yuan, "An evaluation of real-time troposphere estimation based on GNSS precise point positioning," *J. Geophys. Res.*, vol. 122, no. 5, pp. 2779–2790, 2017.

[9] C. Lu *et al.*, "Real-time tropospheric delays retrieved from multi-GNSS observations and IGS real-time product streams," *Remote Sens.*, vol. 9, no. 12, 2008, Art. no. 1317, doi: 10.3390/rs9121317.

[10] A. Bilich and K. M. Larson, "Mapping the GPS multipath environment using the signal-to-noise ratio (SNR)," *Radio Sci.*, vol. 42, no. 6, pp. 1–16, 2007.

[11] A. Bilich, K. M. Larson, and P. Axelrad, "Modeling GPS phase multipath with SNR: Case study from the Salar de Uyuni, Boliva," *J. Geophys. Res. Solid Earth*, vol. 113, no. 4, pp. 1–12, 2008.

[12] C. Rost and L. Wanninger, "Carrier phase multipath corrections based on GNSS signal quality measurements to improve CORS observations," in *Proc. IEEE/ION Position, Location Navigat. Symp.*, May 2010, pp. 1162–1167.

[13] K. M. Larson, E. E. Small, E. Gutmann, A. Bilich, P. Axelrad, and J. Braun, "Using GPS multipath to measure soil moisture fluctuations: Initial results," *GPS Solutions*, vol. 12, no. 3, pp. 173–177, 2008.

[14] K. M. Larson, J. J. Braun, E. E. Small, V. U. Zavorotny, E. D. Gutmann, and A. L. Bilich, "GPS multipath and its relation to near-surface soil moisture content," *IEEE J. Sel. Topics Appl. Earth Observ. Remote Sens.*, vol. 3, no. 1, pp. 91–99, Mar. 2010.

[15] C. C. Chew, E. E. Small, K. M. Larson, and V. U. Zavorotny, "Effects of near-surface soil moisture on GPS SNR data: Development of a retrieval algorithm for soil moisture," *IEEE Trans. Geosci. Remote Sens.*, vol. 52, no. 1, pp. 537–543, Jan. 2014.

[16] G. Foti *et al.*, "Spaceborne GNSS reflectometry for ocean winds: First results from the UK TechDemoSat-1 mission," *Geophys. Res. Lett.*, vol. 42, no. 13, pp. 5435–5441, 2015.

[17] Santamaría-Gómez, C. Watson, M. Gravelle, M. King, and G. Wöppelmann, "Levelling co-located GNSS and tide gauge stations using GNSS reflectometry," *J. Geod.*, vol. 89, no. 3, pp. 241–258, 2015.

[18] J. Strandberg, T. Hobiger, and R. Haas, "Improving GNSS-R sea level determination through inverse modeling of SNR data," *Radio Sci.*, vol. 51, no. 8, pp. 1286–1296, 2016.

[19] O. Roggenbuck, J. Reinking, and T. Lambertus, "Determination of significant wave heights using damping coefficients of attenuated GNSS SNR data from static and kinematic observations," *Remote Sens.*, vol. 11, no. 4, p. 409, 2019.

[20] V. U. Zavorotny, S. Gleason, E. Cardellach, and A. Camps, "Tutorial on remote sensing using GNSS bistatic radar of opportunity," *IEEE Geosci. Remote Sens. Mag.*, vol. 2, no. 4, pp. 8–45, Dec. 2014.

[21] A. Komjathy, V. U. Zavorotny, P. Axelrad, G. H. Born, and J. L. Garrison, "GPS signal scattering from sea surface: Wind speed retrieval using experimental data and theoretical model," *Remote sens. Environ.*, vol. 73, no. 1, pp. 162–174, 2000.

[22] J. L. Garrison, A. Komjathy, V. U. Zavorotny, and S. J. Katzberg, "Wind speed measurement using forward scattered GPS signals," *IEEE Trans. Geosci. Remote Sens.*, vol. 40, no. 1, pp. 50–65, Jan. 2002.

[23] C. S. Ruf *et al.*, "New ocean winds satellite mission to probe hurricanes and tropical convection," *Bull. Amer. Meteorol. Soc.*, vol. 97, no. 3, pp. 385–395, 2016.

[24] K. Emanuel and F. Zhang, "On the predictability and error sources of tropical cyclone intensity forecasts," *J. Atmos. Sci.*, vol. 73, no. 9, pp. 3739–3747, 2016.

[25] C. S. Ruf, S. Gleason, and D. S. McKague, "Assessment of CYGNSS wind speed retrieval uncertainty," *IEEE J. Sel. Topics Appl. Earth Observ. Remote Sens.*, vol. 12, no. 1, pp. 87–97, Jan. 2019.

[26] C. Chew and E. Small, "Soil moisture sensing using spaceborne GNSS reflections: Comparison of CYGNSS reflectivity to SMAP soil moisture," *Geophys. Res. Lett.*, vol. 45, no. 9, pp. 4049–4057, 2018.

[27] L. Michalek, M. Dvorsky, O. Grunt, J. Skapa, and R. Sebesta, "Analysis of signal attenuation in UHF band," *Adv. Electr. Electron. Eng.*, vol. 13, no. 4, pp. 338–343, 2015.

[28] H. Sakoe and S. Chiba, "Dynamic programming algorithm optimization for spoken word recognition," *IEEE Trans. Acoust., Speech, Signal Process.*, vol. ASSP-26, no. 1, pp. 43–49, Feb. 1978.

[29] J. Bemdt and J. Clifford, "Using dynamic time warping to find patterns in time series," in *Proc. 3rd Int. Conf. Knowl. Discovery Data Mining*, 1994, pp. 359–370.

[30] M. Iqbal, R. Tinmaker, and D. M. Chate, "Ligtning activity over India: A study of east-west contrast," *Int. J. Reote Sens.*, vol. 34, no. 16, pp. 5641–5650, 2013.

Saurabh Das (M'10–SM'17) received the Ph.D. degree in radio physics and electronics from the University of Calcutta, Kolkata, India, in 2013. He worked as a Faculty Member with the Indian Statistical Institute, Kolkata, and the University of Calcutta, and as a Research Fellow with the Space Applications Centre, Indian Space Research Organization (ISRO), Ahmedabad, India. He is currently working as an Assistant Professor with the Discipline of Astronomy, Astrophysics and Space Engineering, IIT Indore, Indore, India. His research interest includes radiowave propagation in atmosphere and ionosphere, radar meteorology, Global Navigational Satellite System (GNSS), and machine learning.

Dr. Das has been a Senior Member of IEEE GRSS since 2017.

Soumen Datta received the B.Tech. degree in electronics and communication engineering from Jalpaiguri Government Engineering College, Jalpaiguri, India, in 2011, and the post-graduation degree from the Indian Institute of Engineering Science and Technology, Howrah, India, in 2015. He is currently pursuing the Ph.D. degree in the Discipline of Astronomy, Astrophysics and Space Engineering, with IIT Indore, Indore, India.

He has worked as a Research Fellow with the Indian Statistical Institute, Kolkata, India. His research interests include atmospheric effects on radiowave propagation, remote sensing, and Global Navigational Satellite System (GNSS).

Ashish K. Shukla received the Ph.D. degree in applied mathematics (fluid mechanics) from Lucknow University, Lucknow, India, in 2003.

He joined the Space Applications Centre (SAC), Indian Space Research Organization (ISRO), Ahmedabad, India, as a Scientist, in May 2005. He is working in the field of satellite navigation for more than 13 years and has contributed significantly in satellite navigation programs of ISRO. He has authored more than 25 publications in peer-reviewed journals and proceedings. His research interests include the development of algorithms for Navigation with Indian Constellation (NavIC) and GPS carrier phase-based precise positioning, differential positioning, development of terrestrial positioning algorithms, atmospheric water vapour retrieval using Global Navigational Satellite System (GNSS) signals, and ionospheric modeling.